Muscle and Tendon Tissues: Constitutive Modeling and Computational Issues

L. A. Spyrou
e-mail: lspyrou@mie.uth.gr

N. Aravas[1]
Professor, Fellow ASME
e-mail: aravas@mie.uth.gr

Department of Mechanical Engineering,
University of Thessaly,
38334 Volos, Greece;
The Mechatronics Institute,
Center for Research and Technology-Thessaly
(CE.RE.TE.TH.),
38500 Volos, Greece

A three-dimensional constitutive model for muscle and tendon tissues is developed. Muscle and tendon are considered as composite materials that consist of fibers and the connective tissues and biofluids surrounding the fibers. The model is nonlinear, rate dependent, and anisotropic due to the presence of the fibers. Both the active and passive behaviors of the muscle are considered. The muscle fiber stress depends on the strain (length), strain-rate (velocity), and the activation level of the muscle, whereas the tendon fiber exhibits only passive behavior and the stress depends only on the strain. Multiple fiber directions are modeled via superposition. A methodology for the numerical implementation of the constitutive model in a general-purpose finite element program is developed. The current scheme is used for either static or dynamic analyses. The model is validated by studying the extension of a squid tentacle during a strike to catch prey. The behavior of parallel-fibered and pennate muscles, as well as the human semitendinosus muscle, is studied. [DOI: 10.1115/1.4003741]

Keywords: skeletal muscle, muscle mechanics, tendon mechanics, biomechanics, finite element modeling, constitutive modeling

1 Introduction

Skeletal muscle is the biological material responsible for the production of force and the movement of the human body. Skeletal muscles exhibit both "active" and "passive" mechanical characteristics. Whereas force-elongation or stress-strain relations can be well defined for bones or ligaments, such relations are not as straightforward for the case of muscle because of its contractile properties. The muscle fiber controls both the active and passive behaviors of the muscle. The active behavior is known to depend on the fiber-length and velocity of contraction, as well as on the activation level of the muscle, whereas the passive behavior depends on the fiber-length, the velocity of passive stretching and/or releasing, and the calcium level. From a macroscopic "continuum" point of view, this means that the stresses in the muscle depend on the local strain, strain rate, and activation level.

The development of realistic constitutive models for the mechanical behavior of the muscle tissue improves our basic understanding of the complex muscle function. Such models, combined with advanced imaging techniques (computed tomography and magnetic resonance imaging), form the basis for realistic simulation of the human musculoskeletal system.

The available constitutive models for the mechanical behavior of muscles can be divided in three main categories: (a) cross-bridge models, (b) one-dimensional Hill-type three-component models, and (c) three-dimensional continuum models.

The one-dimensional character and the lack of consideration of the microstructural muscle characteristics of the cross-bridge [1] and the Hill-type models limit their applicability to realistic three-dimensional muscle systems. In the last decade, several attempts have been made toward the development of more realistic three-dimensional constitutive equations for muscle and tendon [2–9].

In the present paper, we develop a continuum constitutive model for muscle and tendon tissues using an approach similar to that of Liang et al. [9], who developed a model for muscular hydrostats. Muscle and tendon tissues are treated as composite materials that consist of the fibers and the connective tissues and biofluids surrounding the fibers. The stress in the muscle fiber has an active and a passive part. The model accounts for the dependence of the active fiber force on the fiber-length, fiber-velocity, and activation level of the muscle, i.e., the active fiber stress is a function of the fiber strain, strain-rate, and the activation level. The maximum active fiber force appears at the so-called "optimal fiber-length," which is known to depend on the activation level. The corresponding passive fiber stress depends on the fiber strain and the activation level; when the muscle is not active, the fiber stress depends also on strain-rate (see Eq. (3) below).

The model accounts for the dependence of the optimal fiber-length on the activation level, and includes both strain-rate and calcium level effects on muscle fiber's passive tension. The nominal muscle fiber stress σ_0^m is written in the form

$$\sigma_0^m = \sigma_0^{m(\mathrm{act})} + \sigma_0^{m(\mathrm{pas})} \tag{1}$$

with

$$\sigma_0^{m(\mathrm{act})} = \sigma_{\max} f_a f_e(\varepsilon_0^m, f_a) f_r(\dot{\varepsilon}_0^m) \tag{2}$$

and

$$\sigma_0^{m(\mathrm{pas})} = \begin{cases} \sigma_{\max} f_p(\varepsilon_0^m, f_a), & f_a > 0 \\ \sigma_{\max} f_p(\varepsilon_0^m) f_{pr}(\dot{\varepsilon}_0^m), & f_a = 0 \end{cases} \tag{3}$$

where $\sigma_{\max}$ is the reference stress, f_a is the activation level, $(\varepsilon_0^m, \dot{\varepsilon}_0^m)$ is the fiber nominal strain and strain-rate, and (f_e, f_r, f_p, f_{pr}) are the dimensionless functions.

The resulting constitutive model for the muscle is nonlinear, anisotropic, and rate dependent (viscoelastic). Tendons are treated as passive materials in which stress is a nonlinear function of the corresponding strain.

A methodology for the numerical implementation of the resulting constitutive equations in a general-purpose finite element program (ABAQUS) is developed. The constitutive model is then used to study the behavior of several muscle-tendon systems.

Standard notation is used throughout. Boldface symbols denote tensors, the orders of which are indicated by the context. The

[1]Corresponding author.

Contributed by the Applied Mechanics Division of ASME for publication in the JOURNAL OF APPLIED MECHANICS. Manuscript received October 28, 2010; final manuscript received February 28, 2011; accepted manuscript posted March 2, 2011; published online April 14, 2011. Editor: Robert M. McMeeking.

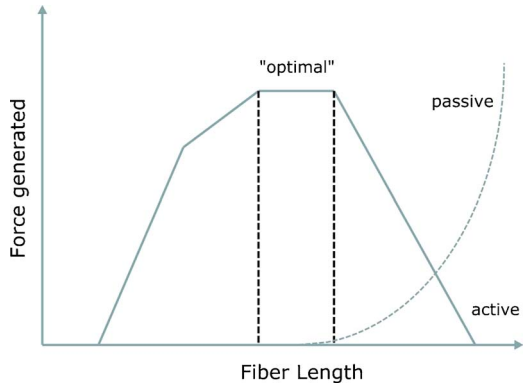

Fig. 1 A typical force-length relation for skeletal muscle fiber

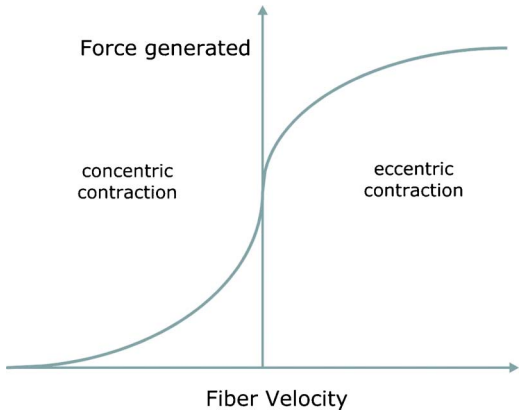

Fig. 2 A typical active force-velocity relation for skeletal muscle fiber

usual summation convention is used for repeated Latin indices of tensor components with respect to a fixed Cartesian coordinate system with base vectors $\mathbf{e}_i (i=1,2,3)$. The preface "det" indicates the determinant, a superscript T indicates the transpose, and a superposed dot indicates the material time derivative. Let **a**, **b**, **c**, and **d** be the vectors, **A** and **B** be the second-order tensors, and **C** and **D** be the fourth-order tensors; the following products are used in the text: $(\mathbf{ab})_{ij}=a_i b_j$, $(\mathbf{abcd})_{ijkl}=a_i b_j c_k d_l$, $(\mathbf{a}\cdot\mathbf{A})_i=a_j A_{ji}$, $(\mathbf{A}\cdot\mathbf{a})_i=A_{ij}a_j$, $(\mathbf{a}\cdot\mathbf{A}\cdot\mathbf{a})_{ij}=a_i A_{ij} a_j$, $\mathbf{A}:\mathbf{B}=A_{ij}B_{ij}$, $(\mathbf{A}:\mathbf{C})_{ij}=A_{kl}C_{klij}$, $(\mathbf{C}:\mathbf{A})_{ij}=C_{ijkl}A_{kl}$, and $(\mathbf{C}:\mathbf{D})_{ijkl}=C_{ijpq}D_{pqkl}$.

2 Mechanical Behavior of Skeletal Muscles

The basic function of muscle is its ability to produce force and its capability of active contraction makes it distinct from other soft biological tissues. Muscles perform both dynamic and static works. Dynamic work permits locomotion and the positioning of the body segments in space, whereas static work maintains body posture and position.

The force developed by a muscle during contraction varies with its fibers' length, velocity, and level of activation [10,11]. The force is also dependent on the fiber arrangement in the muscle (i.e., parallel, and pennate) and the fiber type (i.e., slow-twitch and fast-twitch).

Active force-length relations are obtained experimentally under isometric conditions (constant fiber-length) and for maximal activation of the muscle. Isometric contractions are performed at different fiber-lengths and the peak isometric force is measured at each length. These forces are then plotted against length and a relationship such as that labeled "active" in Fig. 1 is obtained [12].

It has been demonstrated that at very long and very short lengths, muscle generates a low force whereas at intermediate "optimal" lengths, muscle generates a higher force. At the microstructural level, the force-length relationship illustrates that force generation in skeletal muscle is a direct function of the magnitude of overlap between the actin and myosin filaments [13].

Passive force is developed if a muscle fiber is stretched to various lengths without stimulation. In general, when the length of a muscle fiber is less than the optimal, the passive force is almost zero. The passive force increases as the muscle fiber is stretched beyond its optimal length (Fig. 1). These relatively long lengths can be attained physiologically, and passive tension can play a role in providing resistive force even in the absence of muscle activation. Apart from the intramuscular connective tissue (epimysium, perimysium, and endomysium), which adds to the elasticity of the muscle, the large protein titin, which connects the thick myosin filaments end to end, has been identified as the main source of this passive tension [14].

Active force-velocity relations show the dependence of the maximum force a muscle can exert on the rate of change of its length. These relations are obtained for maximal activation of the muscle and "optimal" fiber-length. Experimentally, a muscle fiber is stimulated maximally and allowed to shorten (or lengthen) against a constant load. The velocity of the fiber end during shortening (or lengthening) is measured and plotted against the resistive force. A general form of this relationship is shown in Fig. 2 [12].

From the mechanical point of view, the force-velocity curve provides the relation between stress and strain-rate and defines the "viscoelastic" properties of skeletal muscle for shortening and stretch contractions.

The force-velocity relationship is obtained at "optimal" fiber-lengths. That relation can be generalized for "nonoptimal" fiber-lengths by using a relationship of the form [15]

$$F = f(v)g(\ell) \tag{4}$$

where F is the muscle force, $f(v)$ is a normalized force-velocity function, and $g(\ell)$ is a normalized force-length function.

Additional passive force-velocity characteristics are developed when a nonactivated muscle fiber is stretched above its optimal length and/or released [16,17]. When the rate of passive stretching (or releasing) is increased, the material's behavior becomes stiffer.

Force-activation relations show the dependence of the active force a muscle can generate on the level of activation. The primal role of activation level is to adjust the magnitude of the active force. An interrelation between the level of activation and the active force-length properties has been identified. It has been shown that optimal fiber-lengths increase as activation decreases [18,19]. The level of activation also affects the passive behavior of a muscle, i.e., when a stretch is imposed on a contracting muscle. Experiments with muscle fibers showed that calcium addition resulted in titin-based tension increase and thus passive force enhancement [20,21].

3 Brief Review on Tendon Mechanics

In contrast to muscles, tendons exhibit only passive behavior. Their primal role is to transmit the force of their associated muscle to the bone. The force-length relationship in uniaxial tension is of the form shown in Fig. 3 [22]. Three distinct regions can be identified on the curve shown in Fig. 3.

In region I, known as the "toe" region, a nonlinear behavior of the material is observed; this is caused mainly by the straightening of the collagen crimp. In region II, known as the "linear" region, the aligned collagen fibers are stretched until some of them start to break. Further tendon loading increases dramatically the fracture of the fibers (region III or "yield" region). Stretching beyond region III causes complete failure of the tendon.

The force-elongation curve shown in Fig. 3 defines the corresponding stress-strain curve in uniaxial tension, which is then

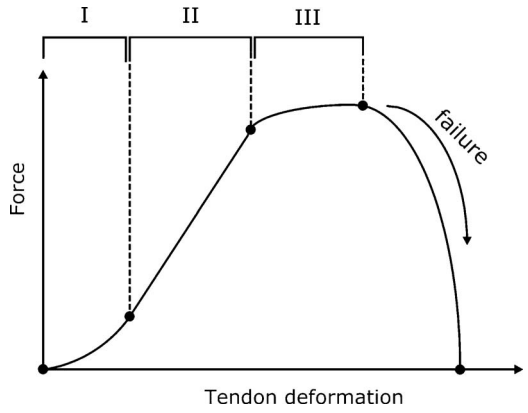

Fig. 3 A typical force-deformation relation for tendon tissue

used to specify Young's modulus, the ultimate stress, and the ultimate strain of tendon tissue. The slope of the stress-strain curve in the "linear" region is usually used to define Young's modulus, which takes values in the range 1–2 GPa [23]. The corresponding ultimate stress and ultimate nominal strain are of the order of 100 MPa and 4–10%, respectively [23].

4 The Constitutive Model

The structural unit of skeletal muscle is the muscle fiber, which is composed of parallel bundles of myofibrils. Each myofibril is divided longitudinally by the Z-disks into sarcomeres, which are the basic contractile units of a muscle. The sarcomeres are also responsible for the passive properties of the muscle.

The structural unit of tendon is the collagen fiber. Tendons exhibit passive behavior only.

Both muscle and tendon are essentially composite materials that consist of fibers and the connective tissue and biofluids surrounding the fibers. In the present approach, muscle and tendon are viewed as anisotropic composite continuous media and a "homogenization" scheme is used in order to derive the constitutive equations that describe their mechanical behavior. The resulting constitutive models are nonlinear and the anisotropy is defined locally in terms of the local fiber direction as described in the following. The constitutive model for the muscle is also rate dependent and accounts for the influence of fiber contraction velocity on the muscle force, as shown in Fig. 2.

At every material point in the tissue, the local direction of the *deformed* fiber is defined by the corresponding unit vector $\mathbf{m}$ (Fig. 4). Let $\mathbf{F}$ be the value of the deformation gradient at a material point. Then the unit vector $\mathbf{m}$ at that point can be determined from

$$\mathbf{m} = \frac{1}{|\mathbf{F}\cdot\mathbf{m}_0|}\mathbf{F}\cdot\mathbf{m}_0 \tag{5}$$

where $\mathbf{m}_0$ is the unit vector that defines the orientation of the fiber in the undeformed configuration.

We consider the Eulerian logarithmic strain tensor:

$$\boldsymbol{\varepsilon} = \ln \mathbf{V} \equiv \sum_{i=1}^{3} \ln \lambda_i \mathbf{n}_i \mathbf{n}_i \tag{6}$$

where $\mathbf{V} = \sqrt{\mathbf{F}\cdot\mathbf{F}^T} \equiv \Sigma_{i=1}^{3}\lambda_i \mathbf{n}_i\mathbf{n}_i$, the principal stretches λ_i are the eigenvalues of $\mathbf{V}$, and $\mathbf{n}_i$ are the eigenvectors of $\mathbf{V}$.

Let $\boldsymbol{\varepsilon}^f$ be the part of the strain tensor associated locally with the volume preserving axial local deformation in the direction $\mathbf{m}$ of the fiber. The change of length of an infinitesimal fiber segment of original length ds_0 can be determined in terms of the corresponding stretch ratio λ_m:

$$\lambda_m = \frac{ds}{ds_0} = \sqrt{\mathbf{m}_0\cdot\mathbf{F}^T\cdot\mathbf{F}\cdot\mathbf{m}_0} \tag{7}$$

where ds is the length of the infinitesimal fiber segment after the deformation. The associated axial logarithmic strain in the fiber direction is ε_m:

$$\varepsilon_m = \ln \lambda_m \tag{8}$$

The rate of change of ε_m can be determined as

$$\dot{\varepsilon}_m = \frac{\dot{\lambda}_m}{\lambda_m} = \mathbf{m}\cdot\mathbf{D}\cdot\mathbf{m} \tag{9}$$

where $\mathbf{D}$ is the deformation rate tensor defined as the symmetric part of the spatial velocity gradient in the deformed configuration.[2]

In the following, we use a kinematics approach similar to that of Liang et al. [9] in order to describe the strain tensor in the tissue. The corresponding volume preserving logarithmic fiber strain tensor can be written as

$$\boldsymbol{\varepsilon}^f = \varepsilon_m \mathbf{m}\mathbf{m} - \frac{\varepsilon_m}{2}(\mathbf{e}_1\mathbf{e}_1 + \mathbf{e}_2\mathbf{e}_2) \tag{10}$$

where $\mathbf{e}_1$ and $\mathbf{e}_2$ are the unit vectors such that $(\mathbf{e}_1, \mathbf{e}_2, \mathbf{m})$ form a right-handed orthonormal basis. Taking into account that $\mathbf{e}_1\mathbf{e}_1 + \mathbf{e}_2\mathbf{e}_2 + \mathbf{m}\mathbf{m} = \boldsymbol{\delta}$, we conclude that Eq. (10) can be written in the form

$$\boldsymbol{\varepsilon}^f = \frac{\varepsilon_m}{2}(3\mathbf{m}\mathbf{m} - \boldsymbol{\delta}) \tag{11}$$

where $\boldsymbol{\delta}$ the second-order identity tensor.

The difference between the total strain $\boldsymbol{\varepsilon}$ and the fiber strain $\boldsymbol{\varepsilon}^f$ is associated with the connective tissue and the biofluids surrounding the fibers:

$$\boldsymbol{\varepsilon}^{ct} = \boldsymbol{\varepsilon} - \boldsymbol{\varepsilon}^f \tag{12}$$

In particular, $\boldsymbol{\varepsilon}^{ct}$ represents the extent to which the total strain is locally not axisymmetric with respect to the fiber and is not volume preserving; i.e., it represents any area change transverse to the muscle fiber due to a local volume change in the "composite" material and any local transverse and axial shear relative to the fiber.

If the fiber strain (10) were the only strain in the tissue, then the corresponding local true stress tensor would be a uniaxial stress in the local direction of the fiber (Fig. 4), i.e.,

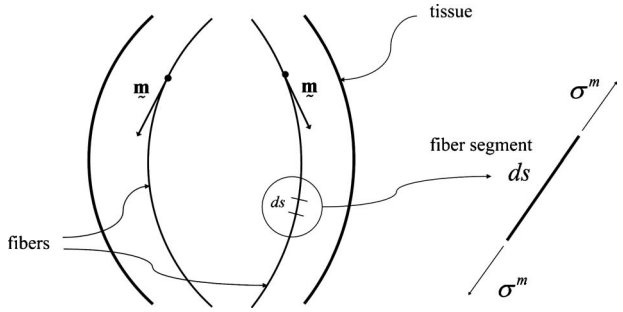

Fig. 4 Tissue fiber in the deformed configuration with its direction defined locally by unit vector m. Also shown the fiber stress σ_m acting on an infinitesimal fiber segment of length *ds*.

[2]Equation (9) leads to the more involved formula for the evaluation of ε_m, which is used sometimes incrementally in computational mechanics: $d\varepsilon_m = \mathbf{m}\cdot\mathbf{D}\cdot\mathbf{m}dt$ or $\varepsilon_m(t) = \int_0^t \mathbf{m}(\tau)\cdot\mathbf{D}(\tau)\cdot\mathbf{m}(\tau)d\tau$, where t denotes time.

$$\boldsymbol{\sigma}^f = \sigma^m \mathbf{mm} \tag{13}$$

where σ^m is the true stress in the fiber direction and depends on the fiber strain and strain-rate as described in the following.

In the general case, additional stresses $\boldsymbol{\sigma}^{ct}$ develop due to the deformation $\boldsymbol{\varepsilon}^{ct}$ of the connective tissues and the biofluids.

As a first approximation, we assume that the total true stress $\boldsymbol{\sigma}$ in the tissue can be written as the sum of $\boldsymbol{\sigma}^f$ and $\boldsymbol{\sigma}^{ct}$:

$$\boldsymbol{\sigma} = \boldsymbol{\sigma}^f + \boldsymbol{\sigma}^{ct} \tag{14}$$

where $\boldsymbol{\sigma}^f$ and $\boldsymbol{\sigma}^{ct}$ depend on the deformation of the tissue as described in the following.

4.1 Constitutive Description of the Fiber Stress σ^m. The nominal strain in the fiber ε_0^m is defined as

$$\varepsilon_0^m = \frac{ds - ds_0}{ds_0} = \lambda_m - 1 = \exp(\varepsilon_m) - 1 \tag{15}$$

so that

$$\varepsilon_m = \ln(1 + \varepsilon_0^m) \tag{16}$$

The nominal axial stress σ_0^m in the fiber is defined in terms of the true fiber stress σ^m as follows:

$$\sigma_0^m = \sigma^m \frac{A}{A_0} = \sigma^m \frac{ds_0}{ds} = \frac{\sigma^m}{\lambda_m} = \frac{\sigma^m}{1 + \varepsilon_0^m} \tag{17}$$

where A and A_0 denote the current and reference cross-sectional area of the fiber respectively. In deriving the last equation, we took into account that, in view of the incompressibility of the fibers, $A_0 ds_0 = A ds$.

4.1.1 The Muscle Fiber Stress. The total nominal longitudinal stress in a muscle fiber is a function of the nominal longitudinal strain ε_0^m, the nominal longitudinal strain-rate $\dot{\varepsilon}_0^m$, and the activation level. Using an approach similar to that of Van Leeuwen and Kier [24], who studied the mechanics of muscular hydrostats, we write a general expression for the fiber stress in the form

$$\sigma_0^m = f(\varepsilon_0^m, \dot{\varepsilon}_0^m, f_a) \tag{18}$$

where f_a is the activation level of the muscle.

The force exerted by a muscle fiber has "active" and "passive" characteristics. The active part of the force depends on the activation level, the fiber-length, and the contraction velocity of the muscle fiber; the passive part depends on the length of the muscle fiber, the activation level, and the velocity of the passive stretching and/or releasing.

The nominal longitudinal stress in a muscle fiber is written as the sum of an active and a passive part:

$$\sigma_0^m = \sigma_0^{m(\mathrm{act})} + \sigma_0^{m(\mathrm{pas})} \tag{19}$$

In the following, we use the force-activation, force-length, and force-velocity characteristics of muscle fibers mentioned in Sec. 2 to derive constitutive equations for σ_0^m. In deriving the constitutive relations, we take into account the following:

1. The magnitude of the active force in the active force-length and active force-velocity relationships (Figs. 1 and 2) depends on the level of activation.
2. The active force-velocity relationship for the optimal fiber-length shown in Fig. 2 can be generalized for all fiber-lengths via Eq. (4).
3. The optimal fiber-length depends on the level of activation (Fig. 5).
4. The passive tension is calcium-dependent (Fig. 12).
5. The passive part exhibits viscoelastic behavior.

Following Van Leeuwen and Kier [24], we write

$$\sigma_0^{m(\mathrm{act})} = \sigma_{\max} f_a f_e(\varepsilon_0^m, f_a) f_r(\dot{\varepsilon}_0^m) \tag{20}$$

and

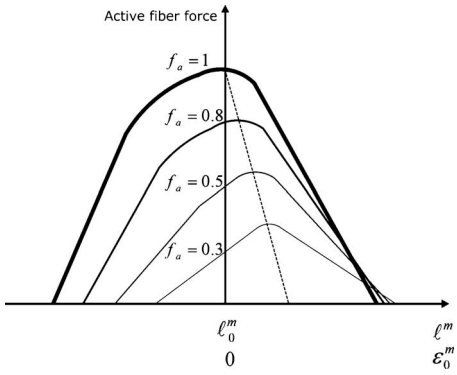

Fig. 5 Active fiber force versus fiber-length at different activation levels [26]. The dash line indicates the location of the maximum force on each curve.

$$\sigma_0^{m(\mathrm{pas})} = \begin{cases} \sigma_{\max} f_p(\varepsilon_0^m, f_a), & f_a > 0 \\ \sigma_{\max} f_p(\varepsilon_0^m) f_{pr}(\dot{\varepsilon}_0^m), & f_a = 0 \end{cases} \tag{21}$$

where f_a is the activation level that controls the magnitude of $\sigma_0^{m(\mathrm{act})}$ and takes values in the range $0 \le f_a \le 1$, f_e describes the dependence of the active stress on the nominal longitudinal strain ε_0^m and accounts for the variation of the optimal fiber-length on the activation level, f_r is the function that relates the active muscle stress to the nominal longitudinal strain-rate $\dot{\varepsilon}_0^m$, f_p describes the dependence of the passive stress on the nominal longitudinal strain ε_0^m and the activation level, and f_{pr} is the function that relates the passive muscle stress to the nominal longitudinal strain-rate $\dot{\varepsilon}_0^m$. In the above equations, $\sigma_{\max}$ is the maximum active isometric stress at optimum fiber-length and the functions (f_e, f_r, f_p, f_{pr}) are all dimensionless and normalized so that

$$\max_{\varepsilon_0^m} f_e(\varepsilon_0^m, f_a) = f_e(\varepsilon_{0a}^m, f_a) = 1 \quad \text{and} \quad f_r(0) = 1 \tag{22}$$

where ε_{0a}^m is the value of the nominal strain that corresponds to the optimal fiber-length at the activation level f_a. In Eq. (20), the nominal fiber strain ε_0^m is defined relative to the optimal fiber-length ℓ_0^m at full activation ($f_a = 1$), i.e.,

$$\varepsilon_0^m = \frac{\ell^m - \ell_0^m}{\ell_0^m} \tag{23}$$

where ℓ^m is the deformed fiber-length. According to the definition of the optimal fiber-length ℓ_0^m and the normalization mentioned above, we have that $f_e = 1$ when $\ell^m = \ell_0^m$ (or $\varepsilon_0^m = 0$) and $f_a = 1$. Therefore, $\varepsilon_{0a}^m = 0$ for $f_a = 1$, i.e.,

$$\max_{\varepsilon_0^m} f_e(\varepsilon_0^m, 1) = f_e(0, 1) = 1 \tag{24}$$

The functions f_e, f_r, f_p, and f_{pr} in Eqs. (20) and (21) are defined based on the mechanical characteristics of the muscle fiber under consideration. The functional form of f_e and f_r are obtained from active force-length and force-velocity experimental data, whereas the functional forms of f_p and f_{pr} are obtained from passive force-length and force-velocity experimental data.

It should be noted that in our approach f_e depends explicitly on the activation state, since the optimal fiber-length ℓ_{0a}^m (the fiber-length that generates the higher force) is known to decrease with increasing activation [18,19]. Figure 5 shows a schematic representation of the variation of the active fiber force with the fiber-length at various activation levels.

The dash line in Fig. 5 indicates the location of the maximum force on each curve and defines the optimal fiber-length as function of the activation level. Lloyd and Besier [25] suggested a relationship of the following form for ℓ_{0a}^m:

$$\ell_{0a}^m(f_a) = \ell_0^m + k(1-f_a)\ell_0^m \tag{25}$$

where ℓ_0^m is the optimal fiber-length at maximum activation ($\ell_{0a}^m = \ell_0^m$ for $f_a=1$) and the constant k defines the maximum optimal fiber-length at zero activation ($\ell_{0a}^m=(1+k)\ell_0^m$ for $f_a=0$). Equations (23) and (25) imply that the maximum fiber stress appears at a nominal strain level ε_{0a} defined by

$$\varepsilon_{0a}^m(f_a) = \frac{\ell_{0a}^m(f_a) - \ell_0^m}{\ell_0^m} = k(1-f_a) \tag{26}$$

In our approach, f_p depends explicitly on the activation state, since the passive tension of the muscle fiber is known to increase with calcium level [20,21]. We suggest a relationship of the following form for f_{pa}:

$$f_{pa}(\varepsilon_0^m) = f_p(\varepsilon_0^m, f_a) = (1+cf_a)f_p(\varepsilon_0^m) \tag{27}$$

where $f_p(\varepsilon_0^m)$ is the function that relates the passive tension with the nominal longitudinal strain ε_0^m at zero activation level ($f_{pa}(\varepsilon_0^m)=f_p(\varepsilon_0^m)$ for $f_a=0$) and the constant c defines the passive tension at maximum activation ($f_{pa}(\varepsilon_0^m)=(1+c)f_p(\varepsilon_0^m)$ for $f_a=1$).

4.1.2 The Tendon Fiber Stress. Tendons develop only "passive" stresses. The passive force depends only on the length of tendon fiber, and the total nominal longitudinal stress in a tendon fiber can be written as a function of the nominal longitudinal strain:

$$\sigma_0^{m(\text{pas})} = \sigma_{\max} f_p^{\text{tend}}(\varepsilon_0^m) \tag{28}$$

where f_p^{tend} is a dimensionless function and $\sigma_{\max}$ is the reference stress introduced in Eq. (20). The tendon strain is defined by the amount of tendon stretch relative to its resting, or slack length, i.e., the length at which the tendon begins to transmit force when stretched [12].

4.2 Constitutive Description of $\boldsymbol{\sigma}^{ct}$. The stress $\boldsymbol{\sigma}^{ct}$ associated with the connective tissue and the biofluids surrounding the fibers is related to the associated logarithmic strain $\boldsymbol{\varepsilon}^{ct}$ through an isotropic, linear hyperelastic equation of the form

$$\boldsymbol{\sigma}^{ct} = \frac{1}{J}\mathcal{L}^e : \boldsymbol{\varepsilon}^{ct} \tag{29}$$

where $J=\det \mathbf{F}$ and $\mathcal{L}^e$ is the fourth-order elasticity tensor defined as

$$\mathcal{L}^e = 2\mu\mathbf{K} + 3\kappa\mathbf{J} \tag{30}$$

with μ and κ being the elastic shear and bulk moduli, respectively. In the last equation, $\mathbf{J}$ and $\mathbf{K}$ are the fourth-order deviatoric and spherical projection tensors defined by

$$\mathbf{J} = \tfrac{1}{3}\boldsymbol{\delta}\boldsymbol{\delta}, \quad \mathbf{K} = \mathbf{I} - \mathbf{J} \tag{31}$$

where $\mathbf{I}$ is the fourth-order symmetric identity tensor with Cartesian components

$$I_{ijkl} = \tfrac{1}{2}(\delta_{ik}\delta_{jl} + \delta_{il}\delta_{jk}) \tag{32}$$

4.3 Summary of Constitutive Equations. The constitutive model developed in Secs. 4.1 and 4.2 can be used also for the case of more that one muscle groups, where different fiber orientations and properties can be incorporated by superposition. In the case of N families of fibers, the constitutive model can be summarized as follows:

$$\mathbf{m}^{(i)} = \frac{1}{|\mathbf{F}\cdot\mathbf{m}_0^{(i)}|}\mathbf{F}\cdot\mathbf{m}_0^{(i)}, \quad \boldsymbol{\varepsilon} = \ln \mathbf{V}, \quad \boldsymbol{\varepsilon} = \boldsymbol{\varepsilon}^f + \boldsymbol{\varepsilon}^{ct} \tag{33}$$

$$\boldsymbol{\sigma} = \boldsymbol{\sigma}^f + \boldsymbol{\sigma}^{ct}, \quad \boldsymbol{\sigma}^{ct} = \frac{1}{J}\mathcal{L}^e : \boldsymbol{\varepsilon}^{ct} \tag{34}$$

$$\boldsymbol{\varepsilon}^f = \sum_{i=1}^{N} \frac{\varepsilon_m^{(i)}}{2}(3\mathbf{m}^{(i)}\mathbf{m}^{(i)} - \boldsymbol{\delta}), \quad \varepsilon_m^{(i)} = \ln \lambda_m^{(i)} \tag{35}$$

$$\lambda_m^{(i)} = \sqrt{\mathbf{m}_0^{(i)}\cdot\mathbf{F}^T\cdot\mathbf{F}\cdot\mathbf{m}_0^{(i)}}, \quad \varepsilon_0^{m(i)} = \lambda_m^{(i)} - 1 \tag{36}$$

$$\boldsymbol{\sigma}^f = \sum_{i=1}^{N} \sigma^{m(i)}\mathbf{m}^{(i)}\mathbf{m}^{(i)}, \quad \sigma^{m(i)} = (1+\varepsilon_0^{m(i)})\sigma_0^{m(i)} \tag{37}$$

$$\sigma_0^{m(i)} = \sigma_0^{m(i)(\text{act})} + \sigma_0^{m(i)(\text{pas})} \tag{38}$$

$$\sigma_0^{m(i)(\text{act})} = \sigma_{\max}^{(i)}[f_a^{(i)} f_e^{(i)}(\varepsilon_0^{m(i)}, f_a^{(i)}) f_r^{(i)}(\dot{\varepsilon}_0^{m(i)}) \tag{39}$$

$$\sigma_0^{m(i)(\text{pas})} = \begin{cases} \sigma_{\max}^{(i)} f_p^{(i)}(\varepsilon_0^{m(i)}, f_a^{(i)}), & f_a^{(i)} > 0 \\ \sigma_{\max}^{(i)} f_p^{(i)}(\varepsilon_0^{m(i)}) f_{pr}^{(i)}(\dot{\varepsilon}_0^{m(i)}), & f_a^{(i)} = 0 \end{cases} \tag{40}$$

The above constitutive model is nonlinear, rate dependent (viscoelastic), and anisotropic; the anisotropy is defined in terms of the local directions of the muscle fibers in the deformed configuration, i.e., the aforementioned unit vectors $\mathbf{m}^{(i)}$.

5 Numerical Implementation of the Constitutive Model

The constitutive model developed in Sec. 4 was implemented in a finite element program. In view of the nonlinearity and the rate dependence of the model, the finite element solution is developed incrementally. The constitutive calculations are carried out at the element Gauss integration points. At a given Gauss point, the solution $(\mathbf{F}_n, \boldsymbol{\sigma}_n, \varepsilon_0^{m(i)}|_n)$ at time t_n and the deformation gradient $\mathbf{F}_{n+1}$ at time $t_{n+1}=t_n+\Delta t$ are known, and the problem is to determine $(\boldsymbol{\sigma}_{n+1}, \varepsilon_0^{m(i)}|_{n+1})$.

The constitutive calculations at the Gauss points are carried out in the following order:

$$\mathbf{V}_{n+1} = \sqrt{\mathbf{F}_{n+1}\cdot\mathbf{F}_{n+1}^T} = \sum_{i=1}^{3} \lambda_i \mathbf{n}_i\mathbf{n}_i \tag{41}$$

$$\boldsymbol{\varepsilon}_{n+1} = \ln \mathbf{V}_{n+1} = \sum_{i=1}^{3} \ln \lambda_i \mathbf{n}_i\mathbf{n}_i \tag{42}$$

$$\lambda_m^{(i)}|_{n+1} = \sqrt{\mathbf{m}_0^{(i)}\cdot\mathbf{F}_{n+1}^T\cdot\mathbf{F}_{n+1}\cdot\mathbf{m}_0^{(i)}} \tag{43}$$

$$\varepsilon_0^{m(i)}|_{n+1} = \lambda_m^{(i)}|_{n+1} - 1, \quad \varepsilon_m^{(i)}|_{n+1} = \ln \lambda_m^{(i)}|_{n+1} \tag{44}$$

$$\mathbf{m}_{n+1}^{(i)} = \frac{1}{|\mathbf{F}_{n+1}\cdot\mathbf{m}_0^{(i)}|}\mathbf{F}_{n+1}\cdot\mathbf{m}_0^{(i)} \tag{45}$$

$$\boldsymbol{\varepsilon}^f|_{n+1} = \frac{1}{2}\sum_{i=1}^{N} \varepsilon_m^{(i)}|_{n+1}(3\mathbf{m}_{n+1}^{(i)}\mathbf{m}_{n+1}^{(i)} - \boldsymbol{\delta}) \tag{46}$$

$$\boldsymbol{\varepsilon}_{n+1}^{ct} = \boldsymbol{\varepsilon}_{n+1} - \boldsymbol{\varepsilon}_{n+1}^f \tag{47}$$

$$\dot{\varepsilon}_0^{m(i)} = \frac{\varepsilon_0^{m(i)}|_{n+1} - \varepsilon_0^{m(i)}|_n}{\Delta t} \tag{48}$$

$$\sigma_0^{m(i)}|_{n+1} = \sigma_0^{m(i)(\text{act})}|_{n+1} + \sigma_0^{m(i)(\text{pas})}|_{n+1} \tag{49}$$

$$\sigma_{n+1}^{m(i)} = (1+\varepsilon_0^{m(i)}|_{n+1})\sigma_0^{m(i)}|_{n+1} \tag{50}$$

$$\boldsymbol{\sigma}_{n+1}^f = \sum_{i=1}^{N} \sigma_{n+1}^{m(i)}\mathbf{m}_{n+1}^{(i)}\mathbf{m}_{n+1}^{(i)} \tag{51}$$

$$\boldsymbol{\sigma}_{n+1}^{ct} = \frac{1}{\det \mathbf{F}_{n+1}} \mathcal{L}^e : \boldsymbol{\varepsilon}_{n+1}^{ct} \tag{52}$$

$$\boldsymbol{\sigma}_{n+1} = \boldsymbol{\sigma}_{n+1}^{f} + \boldsymbol{\sigma}_{n+1}^{ct} \tag{53}$$

where λ_i^2 and $\mathbf{n}_i$ are the eigenvalues and eigenvectors, respectively, of the left Cauchy–Green tensor $\mathbf{B}_{n+1} = \mathbf{F}_{n+1} \cdot \mathbf{F}_{n+1}^T$.

The constitutive model is implemented in the ABAQUS general-purpose finite element program [27]. This code provides a general interface so that a particular constitutive model can be introduced as a "user subroutine" (UMAT).

The "implicit" version of ABAQUS is used, in which the finite element formulation is based on the weak form of the equilibrium equations, the solution is carried out incrementally, and the discretized nonlinear equations are solved by using Newton's method. The Jacobian of the equilibrium Newton-loop requires the so-called "linearization moduli" of the algorithm that handles the constitutive equations; these moduli are defined in terms of a fourth-order tensor $\mathbf{C}$ that relates the variation of stress $\partial\boldsymbol{\sigma}$ to the variation of strain $\partial\boldsymbol{\varepsilon}$ over the increment under consideration:

$$\partial\boldsymbol{\sigma} = \mathbf{C} : \partial\boldsymbol{\varepsilon} \tag{54}$$

The derivation of $\mathbf{C}$ is lengthy and the details of the derivation are reported in Ref. [28]. Here we note that $\mathbf{C}$ can be approximated by

$$\mathbf{C} \simeq \mathbf{C}^f + \mathbf{C}^{ct} \tag{55}$$

where

$$\mathbf{C}^f = (1 + \varepsilon_0^m)(\sigma_0^m + G)\mathbf{H} + \sigma^m \mathbf{A} \tag{56}$$

$$\mathbf{C}^{ct} = \frac{1}{\boldsymbol{J}} \mathcal{L}^e : \left(\mathbf{I} - \frac{3}{2}\mathbf{H} + \frac{1}{2}\boldsymbol{\delta}\mathbf{mm} - \frac{3}{2}\varepsilon_m \mathbf{A} \right) - \boldsymbol{\sigma}^{ct}\boldsymbol{\delta} \tag{57}$$

with

$$\mathbf{H} = \mathbf{mmmm} \tag{58}$$

$$G = (1 + \varepsilon_0^m)\left(\frac{\partial \sigma_0^m}{\partial \varepsilon_0^m} + \frac{1}{\Delta t} \frac{\partial \sigma_0^m}{\partial \dot{\varepsilon}_0^m} \right) \tag{59}$$

$$A_{ijkl} = \tfrac{1}{2}(\delta_{ik} m_j + \delta_{jk} m_i) m_l + \tfrac{1}{2}(\delta_{il} m_j + \delta_{jl} m_i) m_k - 2H_{ijkl} \tag{60}$$

In Eqs. (55)–(60), all quantities are evaluated at the end of the increment under consideration, i.e., at $t = t_{n+1}$.

It is noted that the fourth-order tensor $\mathbf{C}^f$ has both the "minor" and "major" symmetries, i.e.,

$$C_{ijkl}^f = C_{jikl}^f = C_{ijlk}^f = C_{klij}^f \tag{61}$$

whereas $\mathbf{C}^{ct}$ has only the minor but not the major symmetries, i.e.,

$$C_{ijkl}^{ct} \neq C_{klij}^{ct} \tag{62}$$

It should be noted though that use of the symmetric part of $\mathbf{C}$ in the Jacobian maintains the asymptotic quadratic convergence rate of the Newton scheme.

6 Applications

The developed constitutive model is used to study computationally the behavior of several muscle-tendon systems.

First, the extension of a squid tentacle during the strike to catch prey is simulated. This problem is studied in order to validate the developed code and compare the predictions with available experimental and computational results. The tentacle of a squid consists of a group of muscle fibers in a mass of connective tissue and its constitutive description has the same form as that of skeletal muscle [9,24].

Model problems that involve skeletal muscles are also considered. The behavior of a parallel fibered and a pennate muscle is studied. The model is used also to study the behavior of the human semitendinosus muscle. In all problems, the muscle fibers are assumed to have their optimal length in the undeformed configuration, i.e., $\varepsilon_0^m = 0$ at the start of the analysis.

The finite element calculations are carried out using the ABAQUS general-purpose finite element program [27]. In the case of the squid tentacle, dynamic analysis is carried out, whereas the skeletal muscles are studied under quasi-static conditions. The geometric nonlinearities of the problems are taken into account, i.e., the "finite strain" version of the code is used. Three dimensional four-node tetrahedral or eight-node hexahedral elements are used in the calculations. In all analyses, the correctness of the reported results is verified by carrying out mesh convergence studies. The local directions of the muscle fibers are defined as initial conditions at all Gauss integration points in terms of the local unit vectors $\mathbf{m}_0$.

6.1 Extension of a Squid Tentacle. This problem has been studied experimentally and described in detail by Van Leeuwen and Kier [24]. A computational solution to this problem has been given by Johansson et al. [4] and Liang et al. [9].

The tentacle can be separated in two parts: the stalk and the club. The stalk contains all the muscle activity, whereas the club follows passively stalk's activity. The extension of the tentacle is due to the activation of its extensor muscles, which are arranged in two orthogonal transverse groups. The contraction of the transverse muscle groups in conjunction with the incompressibility of the connective tissue causes the extension of the tentacle in the axial direction. The outermost layer of the tentacle is filled with longitudinal muscle fibers in the axial direction; these longitudinal muscles cover 15% of the tentacle's cross section. The passive behavior of both transverse and longitudinal muscles is responsible for the deceleration of the tentacular strike and finally its termination. The passive stiffness of the longitudinal muscles affects the amount of the final extension.

The stalk is modeled by using the constitutive model described in Sec. 4. The activation function f_a used in the calculations is

$$f_a = \begin{cases} 0 & \text{for } t \leq t_0 \\ \left[\dfrac{1}{2} - \dfrac{1}{2}\cos\dfrac{\pi(t - t_0)}{t_1 - t_0} \right]^q & \text{for } t_0 \leq t \leq t_1 \\ 1 & \text{for } t \geq t_1 \end{cases} \tag{63}$$

where t is time, $t_0 = 0$, $t_1 = 50$ ms, and $q = 25$.

The functions f_e, f_r, and f_p and all material data for the stalk are the same as those used by Liang et al. [9]. It should be noted that f_e and f_p are independent of f_a in this case. The passive stiffness of the longitudinal muscles is four times smaller than that of the transverse muscles [4].

The club is modeled as passive, homogeneous, isotropic, incompressible, and linearly elastic, with a Young modulus 10^3 times that of the connective tissue.

A schematic representation of the finite element mesh of the tentacle and the corresponding muscle groups are shown in Fig. 6.

Figures 7 and 8 show the evolution of the tentacle length and the history of the velocity at the tentacle tip during a strike. The results agree with those of previous works [4,9,24].

6.2 Parallel-Fibered Muscle. A simulation of the behavior of a parallel-fibered muscle is presented in this section. A muscle is called parallel-fibered when its fibers are oriented in the direction of the corresponding tendons. A simplified geometry of a muscle-tendon complex is used. The geometry of the parallel-fibered structure represents ideally the human biceps.

An axisymmetric geometry is used to model the parallel-fibered muscle. The local orientation of the fibers in the undeformed configuration is determined by interpolating between the corresponding directions of the fiber on the axis of symmetry and the outermost fibers on the free surface of the muscle. The undeformed configuration and the finite element mesh are shown in Fig. 9(*a*); the muscle-tendon interfaces are also shown in that picture.

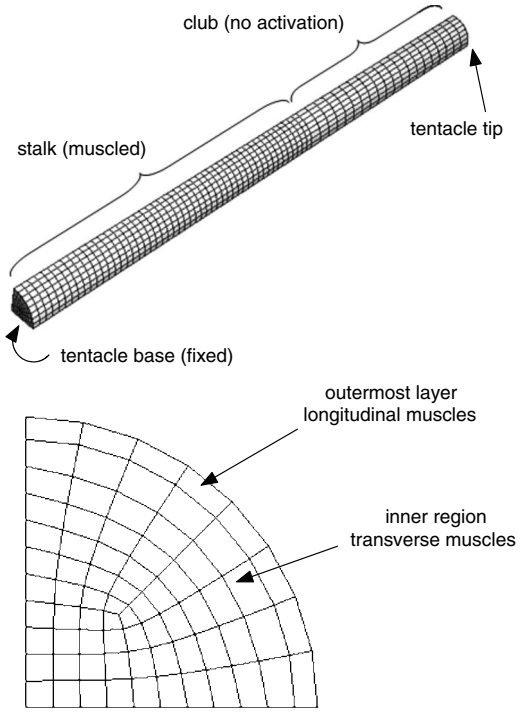

Fig. 6 Up: Finite element mesh used in the calculations. Due to symmetry, only a quarter is analyzed. The tentacle base is constrained in the axial direction and symmetry boundary conditions are imposed to the interior regions. Down: Cross section of the stalk [9]. Longitudinal muscles cover 15% of the tentacle's cross section.

The constitutive model developed in Sec. 4 is used to model the muscle tissue. The maximum active isometric stress at optimum fiber-length $\sigma_{\max}$ takes the value $\sigma_{\max}=300$ kPa. The activation function f_a increases linearly from 0 to 1 over a time period of 1 s and remains constant and equal to unity after that. The constitutive functions $f_e(\varepsilon_0^m)$, $f_r(\dot{\varepsilon}_0^m)$, and $f_p(\varepsilon_0^m)$ are taken from the work of Delp et al. [29] on human lower-extremity muscles; these functions are shown in Figs. 10–12.

The variation of the optimal fiber-length ℓ_{0a}^m with f_a in Fig. 10 is defined by Eq. (25) with $k=0.15$.

The variation of the passive tension f_p with f_a in Fig. 12 is defined by Eq. (27) with $c=0.4$.

The linear hyperelastic behavior of the connective tissue described by Eqs. (29) and (30) is defined by Young's modulus $E=15$ kPa [5] and Poisson's ratio $\nu=0.49995$ (nearly incompressible material).

The tendinous tissue exhibits only passive behavior and is as-

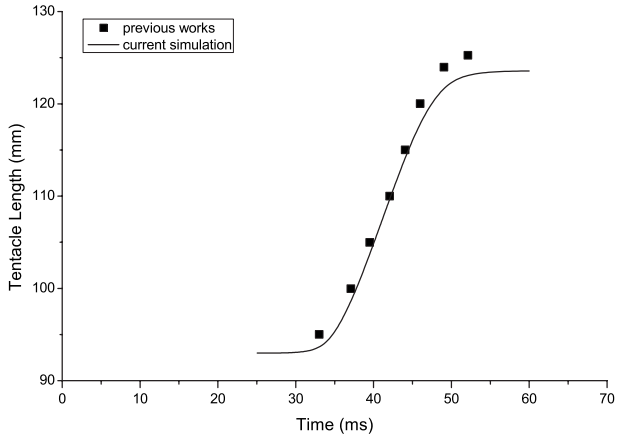

Fig. 7 Evolution of the tentacle length

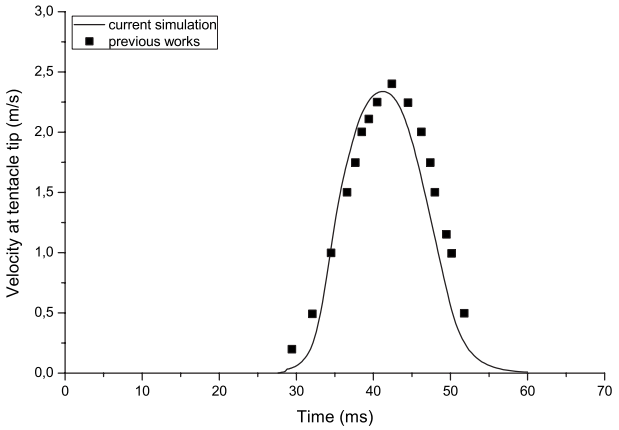

Fig. 8 History of the velocity at the tentacle tip

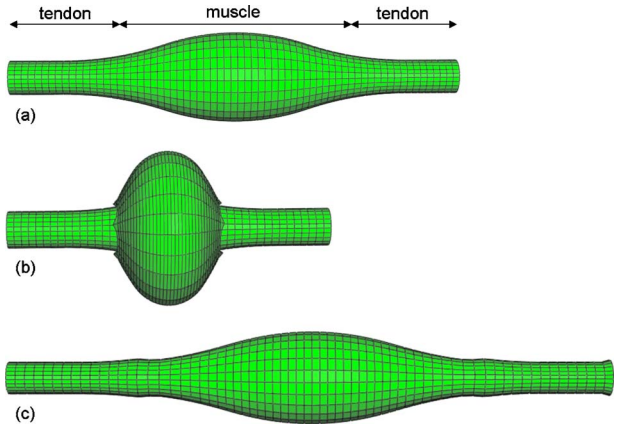

Fig. 9 Parallel-fibered muscle. (*a*) Undeformed configuration. (*b*) Concentric contraction. (*c*) Eccentric contraction.

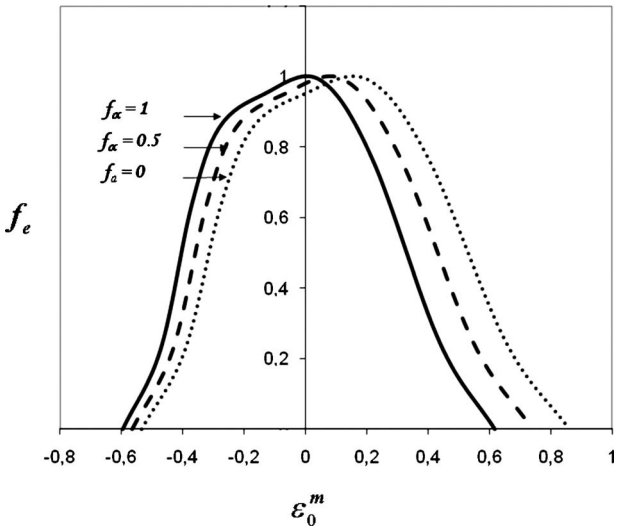

Fig. 10 Dimensionless function f_e versus ε_0^m adopted from Delp et al. [29]. The variation of the optimal fiber-length ℓ_{0a}^m with f_a is considered in the model.

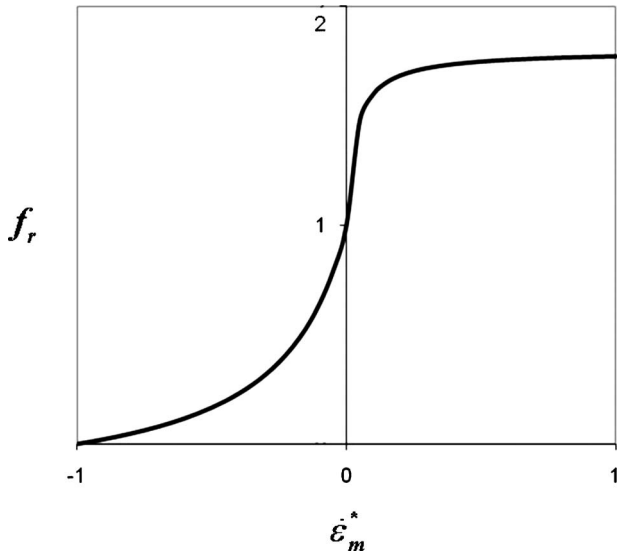

Fig. 11 Dimensionless function f_r versus $\dot{\varepsilon}_m^* = \dot{\varepsilon}_0^m / \dot{\varepsilon}_{max}$, where $\dot{\varepsilon}_{max} = 5\ s^{-1}$ [29]

sumed to be homogeneous, isotropic, and linearly hyperelastic with Young's modulus $E = 100$ MPa and Poisson's ratio $\nu = 0.49995$.

The parallel-fibered muscle is analyzed during concentric and eccentric contraction. In both cases, the activation function f_a is applied for 1 s and one tendon end is constrained in order to eliminate the possibility of rigid body motion. For eccentric contraction, an additional displacement is applied at the other end so that the muscle-tendon structure increases its original length by 25%.

Figure 9 shows the corresponding deformed configurations at the end of the calculation $t = 1$ s. In both cases, the maximum values of the von Mises equivalent stress (measure of shear stresses) and of the hydrostatic stress (measure of normal stresses) appear near the muscle-tendon interfaces, which indicates that these regions are the most susceptible to injuries.

The axial strain in the muscle fiber direction ε_m varies nonuniformly in the muscle volume (Fig. 13). During concentric contraction, the maximum compressive fiber strain ε_m appears at the central region core of the muscle and its value is about 70% larger than that of the outer region and about 300% larger than that of the muscle-tendon interface (Fig. 13(*a*)). The opposite is true in eccentric contraction: The maximum tensile ε_m appears at the muscle-tendon interface and its value is about 300% larger than that of the central region (Fig. 13(*b*)).

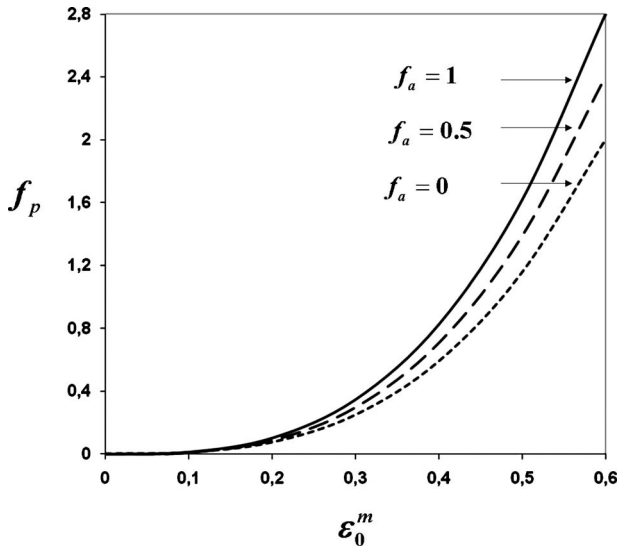

Fig. 12 Passive muscle fiber force-strain relationship adopted from Delp et al. [29]. The variation of the passive tension f_p with f_a is considered in the model.

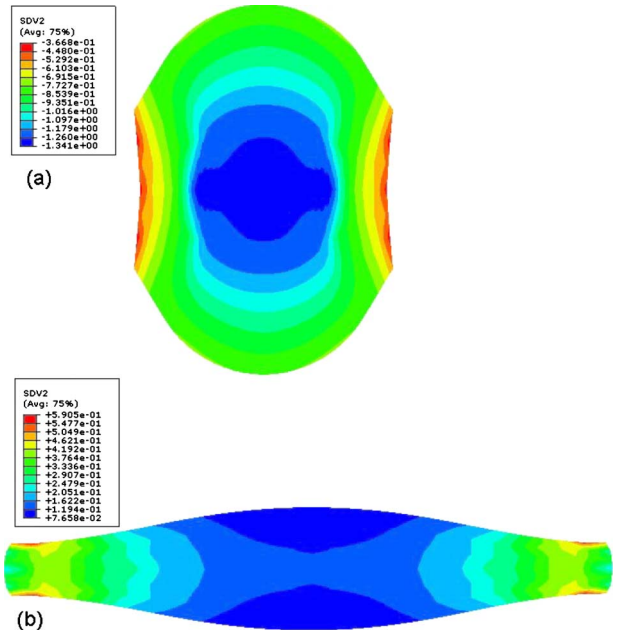

Fig. 13 Contours of fiber strain ε_m in the parallel-fibered muscle. (*a*) Concentric contraction and (*b*) eccentric contraction. The maximum values of ε_m appear at the center of the muscle belly during concentric contraction and at the muscle ends during eccentric contraction.

6.3 Pennate Muscle. A muscle is called pennate when its fibers are oriented at an angle relative to the tendon. A simplified geometry of a muscle-tendon complex is used. In the current application, the muscle fibers are oriented at an angle of 45 deg relative to the tendon. Figure 14(*a*) shows the tendon and muscle parts and the finite element discretization. The material properties for muscle and tendinous tissues are the same as those of the parallel-fibered muscle analyzed in Sec. 6.2.

The pennate muscle is analyzed during concentric and isometric contraction. The duration of both contractions is 1 s. For concentric contraction, the one tendon end is constrained in order to eliminate the possibility of rigid body motion. For isometric contraction, both ends of tendons are fixed so that the total length of the muscle-tendon system remains constant during the analysis.

Figures 14(*b*) and 14(*c*) show the corresponding deformed configurations at the end of the calculations ($t = 1$ s).

In concentric contraction, the fiber shortening is accompanied by an increase in muscle thickness and pennation angle. Also, the axial deformation of the fibers in the central region of the muscle is larger than that in the outer region.

In isometric contraction, the muscle width is increased and the corresponding increase of the thickness is much smaller than that of the concentric contraction. The force transmitted to the muscle-tendon line of action throughout the isometric contraction is two orders of magnitude larger than that of concentric contraction.

6.4 Human Semitendinosus Muscle. The semitendinosus muscle is placed in the thigh area between the pelvis and the knee, and is part of the hamstring muscle group. The semitendinosus muscle helps the extension (straightening) of the hip joint, the flexion (bending) of the knee joint, and the rotation of the knee.

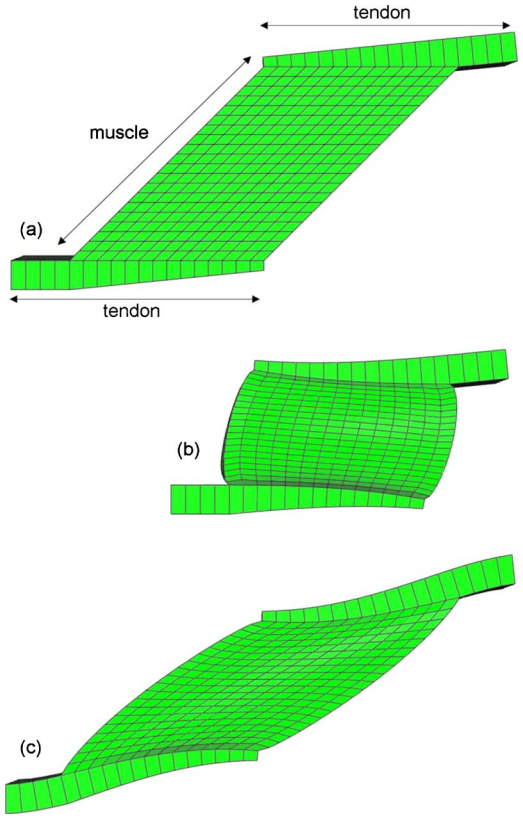

Fig. 14 Pennate muscle. (*a*) Undeformed configuration. (*b*) Concentric contraction. (*c*) Isometric contraction.

The geometry of the muscle is described accurately by using data from MRI scans. Figure 15(*a*) shows the finite element mesh that is based on the MRI data. The material data used for the semitendinosus muscle tissue are the same as those used in Sec. 6.2. The local orientation of the fibers in the undeformed configuration is determined by interpolating between the corresponding directions of the fiber on the outermost fibers on the free surface of the muscle.

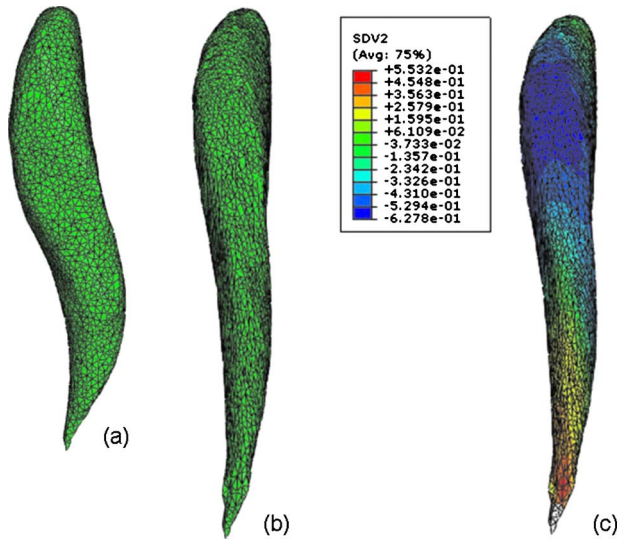

Fig. 15 Human semitendinosus muscle. (*a*) Undeformed configuration and finite element mesh. (*b*) Deformed configuration. (*c*) Contours of axial fiber strain ε_m (fibers that shorten are shown blue).

The analysis is carried out for the eccentric contraction of the muscle. The upper part of the muscle is kept fixed, the activation function increases linearly from 0 to 0.10 (10% activation) in 1 s, and the displacement of the lower end is controlled so that the muscle structure increases its original length by 20%.

Figure 15(*b*) shows the deformed configuration of the semitendinosus muscle at the end of the calculation ($t=1$ s). The deformation is such that the muscle is straightened at the end of the calculation.

Figure 15(*c*) shows the contours of the axial fiber strain ε_m. Despite the increase of the total muscle length and the limited muscle activation of 10%, the upper part experiences shortening contraction and resists the overall extension of the muscle.

7 Closure

The model presented herein can be used for the analysis of muscle-tendon systems under dynamic or quasi-static conditions. The mechanical properties and original orientations of the muscle and tendon fibers are input data. As demonstrated in Sec. 6, the model is capable of predicting the evolution of the muscle shape due to isometric, concentric, or eccentric contraction. The stress and strain fields that develop in complicated muscle systems are also estimated via finite element calculations. Such models, used in conjunction with imaging technology, improve our basic understanding of the mechanical behavior of human muscles and provide an important tool for the simulation of complex muscle systems.

Acknowledgment

This work was carried out while the first author was supported by the "Mechatronics Institute" of the "Center for Research and Development, Thessaly" (CE.RE.TE.TH.). The authors would like to thank Professor R.M. McMeeking of the University of California Santa Barbara for helpful discussions and material. Thanks go also to Professor E. Kellis of the Aristotle University in Greece for providing the geometry of the semitendinosus muscle.

References

[1] Wu, J. Z., Herzog, W., and Cole, G. K., 1997, "Modeling Dynamic Contraction of Muscle Using the Cross-Bridge Theory," Math. Biosci., **139**, pp. 69–78.
[2] Kojic, M., Mijailovic, S., and Zdravkovic, N., 1998, "Modelling of Muscle Behaviour by the Finite Element Method Using Hill's Three-Element Model," Int. J. Numer. Methods Eng., **43**, pp. 941–953.
[3] Martins, J. A. C., Pires, E. B., Salvado, R., and Dinis, P. B., 1998, "A Numerical Model of Passive and Active Behavior of Skeletal Muscles," Comput. Methods Appl. Mech. Eng., **151**, pp. 419–433.
[4] Johansson, T., Meier, P., and Blickhan, R., 2000, "A Finite-Element Model for the Mechanical Analysis of Skeletal Muscles," J. Theor. Biol., **206**, pp. 131–149.
[5] Yucesoy, C. A., Koopman, B. H. F. J. M., Huijing, P. A., and Grootenboer, H. J., 2002, "Three-Dimensional Finite Element Modeling of Skeletal Muscle Using a Two-Domain Approach: Linked Fiber-Matrix Mesh Model," J. Biomech., **35**, pp. 1253–1262.
[6] Lemos, R. R., Epstein, M., Herzog, W., and Wyvill, B., 2004, "A Framework for Structured Modeling of Skeletal Muscle," Comput. Methods Biomech. Biomed. Eng., **7**, pp. 305–317.
[7] Tsui, C. P., Tang, C. Y., Leung, C. P., Cheng, K. W., Ng, Y. F., Chow, D. H. K., and Li, C. K., 2004, "Active Finite Element Analysis of Skeletal Muscle-Tendon Complex During Isometric, Shortening and Lengthening Contraction," Biomed. Mater. Eng., **14**, pp. 271–279.
[8] Blemker, S. S., Pinsky, P. M., and Delp, S. L., 2005, "A 3D Model of Muscle Reveals the Causes of Nonuniform Strains in the Biceps Brachii," J. Biomech., **38**, pp. 657–665.
[9] Liang, Y., McMeeking, R. M., and Evans, A. G., 2006, "A Finite Element Simulation Scheme for Biological Muscular Hydrostats," J. Theor. Biol., **242**, pp. 142–150.
[10] Hill, A. V., 1938, "The Heat of Shortening and the Dynamic Constants of Muscle," Proc. R. Soc., London, Ser. B, **126**, pp. 136–195.
[11] Gordon, A. M., Huxley, A. F., and Julian, F. J., 1966, "The Variation in Isometric Tension With Sarcomere Length in Vertebrate Muscle Fibres," J. Physiol. (London), **184**, pp. 170–192.
[12] Zajac, F. E., 1989, "Muscle and Tendon: Properties, Models, Scaling and Application to Biomechanics and Motor Control," Crit. Rev. Biomed. Eng., **17**, pp. 359–411.

[13] Huxley, A. F., 1957, "Muscle Structure and Theories of Contraction," Prog. Biophys. Biophys. Chem., **7**, pp. 255–318.
[14] Horowits, R., 1992, "Passive Force Generation and Titin Isoforms in Mammalian Skeletal Muscle," Biophys. J., **61**, pp. 392–398.
[15] Epstein, M., and Herzog, W., 1998, *Theoretical Models of Skeletal Muscle: Biological and Mathematical Considerations*, Wiley, New York.
[16] Mutungi, G., and Ranatunga, K. W., 1996, "The Viscous, Viscoelastic and Elastic Characteristics of Resting Fast and Slow Mammalian (Rat) Muscle Fibres," J. Physiol. (London), **496**, pp. 827–836.
[17] Minajeva, A., Neagoe, C., Kulke, M., and Linke, W. A., 2002, "Titin-Based Contribution to Shortening Velocity of Rabbit Skeletal Myofibrils," J. Physiol., **540**, pp. 177–188.
[18] Rack, P. M. H., and Westbury, D. R., 1969, "The Effects of Length and Stimulus Rate on Tension in the Isometric Cat Soleus Muscle," J. Physiol. (London), **204**, pp. 443–460.
[19] Huijing, P. A., 1996, "Important Experimental Factors for Skeletal Muscle Modelling: Non-Linear Changes of Muscle Length Force Characteristics as a Function of Degree of Activity," Eur. J. Morphol., **34**, pp. 47–54.
[20] Labeit, D., Watanabe, K., Witt, C., Fujita, H., Wu, Y., Lahmers, S., Funck, T., Labeit, S., and Granzier, H., 2003, "Calcium-Dependent Molecular Spring Elements in the Giant Protein Titin," Proc. Natl. Acad. Sci. U.S.A., **100**, pp. 13716–13721.
[21] Joumaa, V., Rassier, D. E., Leonard, T. R., and Herzog, W., 2008, "The Origin of Passive Force Enhancement in Skeletal Muscle," Am. J. Physiol.: Cell Physiol., **294**, pp. C74–C78.
[22] Nigg, B. M., and Herzog, W., 1999, *Biomechanics of the Musculo-Skeletal System*, 2nd ed., Wiley, New York.
[23] Maganaris, C. N., Narici, M. V., and Maffulli, N., 2008, "Biomechanics of Achilles Tendon," Disabil Rehabil., **30**, pp. 1542–1547.
[24] Van Leeuwen, J. L., and Kier, W. M., 1997, "Functional Design of Tentacles in Squid: Linking Sarcomere Ultrastructure to Gross Morphological Dynamics," Philos. Trans. R. Soc. London, Ser. B, **352**, pp. 551–571.
[25] Lloyd, D. G., and Besier, T. F., 2003, "An EMG-Driven Musculoskeletal Model for Estimation of the Human Knee Joint Moments Across Varied Tasks," J. Biomech., **36**, pp. 765–776.
[26] Buchanan, T. S., Lloyd, D. G., Manal, K., and Besier, T. F., 2004, "Neuromusculoskeletal Modeling: Estimation of Muscle Forces and Joint Moments and Movements From Measurements of Neural Command," J. Appl. Biomech., **20**, pp. 367–395.
[27] ABAQUS Inc., 2007, ABAQUS Version 6.7 Analysis User's Manual.
[28] Spyrou, L. A., 2009, "Muscle and Tendon Tissues: Constitutive Modeling, Numerical Implementation and Applications," Ph.D. thesis, University of Thessaly, Greece.
[29] Delp, S. L., Peter Loan, J., Hoy, M. G., Zajac, F. E., Topp, E. L., and Rosen, J. M., 1990, "An Interactive Graphics-Based Model of the Lower Extremity to Study Orthopaedic Surgical Procedures," IEEE Trans. Biomed. Eng., **37**, pp. 757–767.